

See discussions, stats, and author profiles for this publication at: <https://www.researchgate.net/publication/372271790>

Surfactin molecules with a cone-like structure promote the formation of membrane domains with negative spontaneous curvature and induce membrane invaginations

Article in *Journal of Colloid and Interface Science* · July 2023

DOI: 10.1016/j.jcis.2023.07.057

CITATIONS

0

READS

25

6 authors, including:



Žiga Pandur

University of Ljubljana

12 PUBLICATIONS 203 CITATIONS

[SEE PROFILE](#)



Samo Penič

University of Ljubljana

36 PUBLICATIONS 282 CITATIONS

[SEE PROFILE](#)



Veronika kralj-iglic

University of Ljubljana

356 PUBLICATIONS 11,189 CITATIONS

[SEE PROFILE](#)

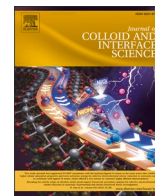
Some of the authors of this publication are also working on these related projects:



No project [View project](#)



mathematical model of the hip [View project](#)



Surfactin molecules with a cone-like structure promote the formation of membrane domains with negative spontaneous curvature and induce membrane invaginations

Žiga Pandur^a, Samo Penič^b, Aleš Iglič^{c,d}, Veronika Kralj-Iglič^e, David Stopar^a, Mitja Drab^{c,d,*}

^a Department of Microbiology, Biotechnical Faculty, University of Ljubljana, 1000 Ljubljana, Slovenia

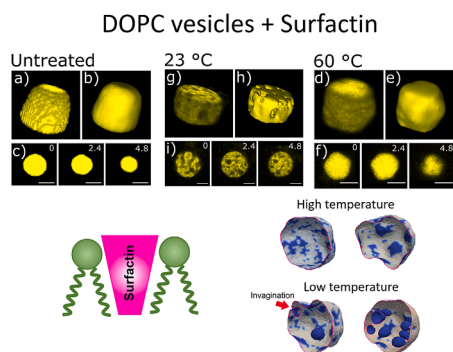
^b Laboratory of Bioelectromagnetics, Faculty of Electrical Engineering, University of Ljubljana, 1000 Ljubljana, Slovenia

^c Laboratory of Physics, Faculty of Electrical Engineering, University of Ljubljana, Ljubljana, Slovenia

^d Laboratory of Clinical Biophysics, Faculty of Medicine, University of Ljubljana, 1000 Ljubljana, Slovenia

^e Laboratory of Clinical Biophysics, Faculty of Health Sciences, University of Ljubljana, 1000 Ljubljana, Slovenia

GRAPHICAL ABSTRACT



ARTICLE INFO

Keywords:

Surfactin
Lipid membranes
Solubilization dynamics
Curved membrane nanodomains
Molecular shape

ABSTRACT

Surfactin uniquely influences lipid bilayer structure by initially inducing membrane invaginations before solubilization. In this study, we exposed DOPC giant vesicles to various surfactin concentrations at different temperatures and observed surfactin-induced membrane invaginations by using differential interference contrast and confocal laser fluorescence microscopy. These invaginations were stable at room temperature but not at higher temperatures. Surfactin molecules induce membrane nanodomains with negative spontaneous curvature and membrane invaginations despite their intrinsic conical shape and intrinsic positive curvature. Considering the experimentally observed capacity of surfactin to fluidize lipid acyl chains and induce partial dehydration of lipid headgroups, we propose that the resulting surfactin-lipid complexes exhibit a net negative spontaneous curvature. We further conducted 3D numerical Monte Carlo (MC) simulations to investigate the behaviour of vesicles containing negative curvature nanodomains within their membrane at varying temperatures. MC simulations demonstrated strong agreement with experimental results, revealing that invaginations are preferentially formed at low temperatures, while being less pronounced at elevated temperatures. Our findings go beyond the

* Corresponding author at: Laboratory of Physics, Faculty of Electrical Engineering, University of Ljubljana, Ljubljana, Slovenia.

E-mail address: mitja.drab@fe.uni-lj.si (M. Drab).

<https://doi.org/10.1016/j.jcis.2023.07.057>

Received 21 January 2023; Received in revised form 22 June 2023; Accepted 9 July 2023

Available online 10 July 2023

0021-9797/© 2023 The Authors. Published by Elsevier Inc. This is an open access article under the CC BY-NC license (<http://creativecommons.org/licenses/by-nc/4.0/>).

expectations of the Israelachvili molecular shape and packing concepts analysis. These concepts do not take into account the influence of specific interactions between neighboring molecules on the inherent shapes of molecules and their arrangement within curved membrane nanodomains. Our work contributes to a more comprehensive understanding of the complex factors governing vesicle morphology and membrane organization and provides insight into the role of detergent-lipid interactions in modulating vesicle morphology.

1. Introduction

Surfactin, derived from *Bacillus subtilis*, is a well-known and powerful bacterial lipopeptide notable for its wide-ranging bioactive characteristics and industrial uses. Exhibiting antibacterial, antifungal, antiviral, antitumor, and insecticidal properties, surfactin also functions as a biosurfactant, a fibrin clot formation inhibitor, an enhancer for oil recovery, and a bioremediation agent [1]. Owing to its multifaceted therapeutic, biotechnological, and commercial attributes, surfactin is an exceptionally versatile biomolecule.

Due to its amphiphilic nature surfactin exerts a strong biological activity in lipid membranes and solubilizes lipids in a highly non-specific manner [2–5]. The large cyclic headgroup of surfactin, comprised of heptapeptides, possesses partial hydrophobic properties, allowing it to penetrate more deeply into the hydrophobic regions of model lipid membranes [6,7]. This likely contributes to its heightened activity and its ability to influence membrane order through chain-tilting effects [8]. Thermodynamic studies using isothermal titration calorimetry on lipid vesicles have revealed distinct differences in behavior between longer bioactive and shorter inactive surfactin homologues [6]. These findings suggest that surfactin strongly interacts with phospholipid acyl chains, resulting in a notable fluidizing effect on the nonpolar portion of the bilayer [3].

Surfactin molecules, which form micelles, generate curvature stress in membranes, leading to lateral disorganization [9]. It has been established that even in a uniformly phased membrane, the packing of amphiphiles is heterogeneous and exhibits an orientational nature [6]. We recently demonstrated that lipid bilayers can experience remarkably intense topological disruptions and exhibit highly non-equilibrium behaviors, enabling the visual examination of vesicle shape deformation dynamics when detergent-to-lipid ratios are meticulously regulated [10]. Furthermore, surfactin has been proven to cause more pronounced lipid destabilization compared to most conventional detergents [8].

In a solution, the surfactin headgroup's peptide ring, which includes two charged amino acid residues, forms a “claw-like” structure that can potentially serve as a binding site for divalent cations, other surfactin molecules, or zwitterionic headgroups of lipids [11]. Furthermore, the intermolecular interactions among surfactin molecules are stronger than those between surfactin and lipids [12], promoting surfactin aggregation into oligomers in the membrane [3,13]. However, this does not mean that surfactin molecules will form one giant aggregate below critical micelle concentration (CMC). Self-assembly of binary mixtures of lipids and detergents is governed by the minimization of the free energy that also includes the contribution of mixing entropy. The composition and size of surfactin-lipid aggregates is influenced by entropy and, through entropy, by temperature. The system's inclination to maximize entropy results in a specific size distribution of surfactin-lipid aggregates at each temperature and concentration [15,16].

A single surfactin molecule or a small cluster exhibits a cone-shaped structure, generating positive curvature stress upon insertion into the lipid bilayer. To accommodate this within the lamellar packing, the molecular mismatch is counterbalanced by lateral headgroup compression (dehydration) and lateral hydrocarbon chain expansion (fluidization). [14]. A surfactin molecule (or their small aggregate) embedded into the lipid bilayer hence influences its immediate surroundings and forms a surfactin-lipid nanodomain that can have net negative spontaneous curvature. Fig. 1 shows a lone surfactin molecule surrounded by fluidized lipids on all sides constituting a surfactin-lipid domain with

negative spontaneous curvature due to the expanded hydrocarbon chains. If such a cluster would include more than one surfactin molecule, the number of negative curvature-promoting lipid molecules on its perimeter would increase proportionally, again resulting in a net negative spontaneous curvature of the surfactin-lipid domain.

Similar effects are known from previous studies of membrane inclusions and embedded intercalated molecules, where the effect of an inclusion can extend up to two or three layers of surrounding lipids [15–1718]. In turn, inclusion-induced curved nanodomains can cluster together and form larger membrane domains with a negative spontaneous curvature, invaginating the membrane inwards on a macroscopic level.

In this study, we showcase the experimental findings on the solubilization dynamics of surfactin in DOPC giant vesicles (GVs) using differential interference contrast (DIC) and confocal laser fluorescence (FL) microscopy techniques. By reconstructing a series of thin-section micrographs, we acquired 3D vesicle images with high spatial and temporal resolution. These visualizations unveiled the emergence of microscale membrane invagination structures before the typical detergent solubilization took place. Additionally, we noted that solubilization

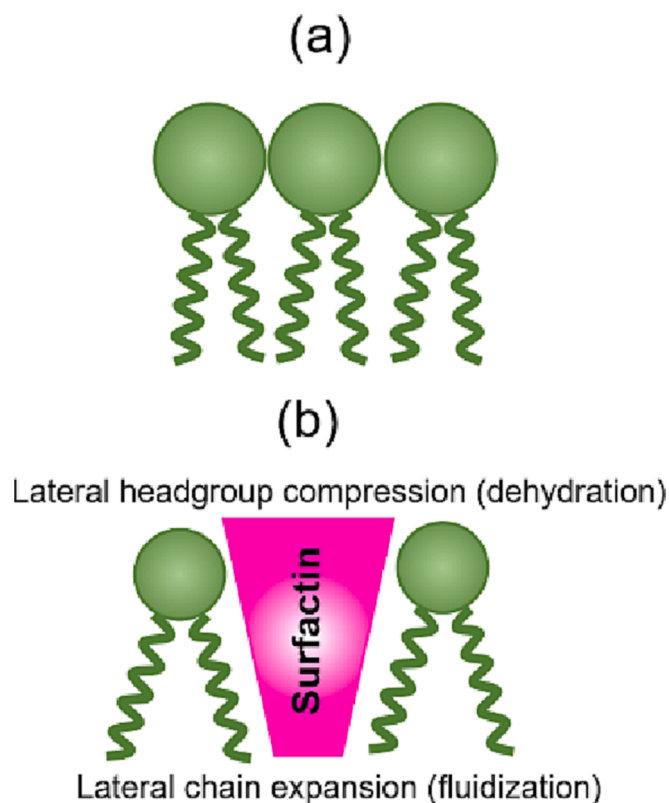


Fig. 1. A schematic representation of an undisturbed outer layer of the lipid bilayer is depicted in (a). The insertion of a cone-shaped surfactin molecule creates a mismatch with the neighboring lipid layers, leading to both dehydration-induced lateral headgroup compression and fluidity-fueled lateral area expansion for each hydrocarbon chain (b) [14,34]. It is important to note that the illustration in (b) demonstrates the most basic scenario of a single embedded surfactin molecule – a cluster of surfactin molecules would similarly impact the curvature of the surfactin-lipid interface.

dynamics were influenced by both concentration and temperature. Specifically, the frequency of vesicle membrane invaginations increased in proportion to surfactin concentration in GV suspensions, although this effect diminished at elevated temperatures.

In addition to conducting experiments, we carried out numerical Monte Carlo simulations to analyze the morphology of closed vesicle shapes with triangulated surfaces. Our basic model allowed for the membrane to have either flat regions devoid of non-zero spontaneous curvature or areas exhibiting negative spontaneous curvature. The simulation outcomes aligned with our experimental findings, indicating a potential mechanism behind the formation of membrane invaginations. Although surfactin molecules possess an inherent positive intrinsic curvature, resembling a conical shape with a wider exterior, they can create membrane domains exhibiting negative spontaneous curvature as a result of headgroup dehydration and lateral chain expansion.

2. Methods

2.1. Preparation of giant lipid vesicles

Giant DOPC lipid vesicles were prepared as described by Moscho et al. [19]. This “gentle hydration method” is known to provide mostly giant unilamellar vesicles as supported by transmission electron microscopy (TEM) [19]. To observe the vesicles with FL, we fluorescently labeled vesicle lumen with a fluorescence dye fluorescein. Fluorescein is a fluorophore commonly used in microscopy, in a type of dye laser as the gain medium, in forensics and serology to detect latent blood stains, and in dye tracing. Fluorescein has an absorption maximum at 494 nm and emission maximum of 512 nm (in water). DOPC was dissolved in chloroform to a concentration of 0.1 M. Then 115 μL of lipid solution was transferred into 250 mL round bottom flask containing 5.6 mL chloroform and 572 μL of methanol. Next, 40 mL of buffer solution (10 mM HEPES buffer, pH = 7.4) with added fluorescein sodium salt (Thermo Fisher Scientific, USA) to a final concentration of 375 mg/mL was carefully added along the flask walls to the lipid solution. Organic solvent was removed with a rotary evaporator (Büchi Rotavapor R-134, Büchi Water bath B-480, Büchi Vacuum Controller V-850, Büchi Vacuum pump V-700) at 40 rpm under reduced pressure (final pressure 55 mbar, volume flow rate 1.8 m^3/h) in a warm water bath (40 °C). Around the evaporation point of chloroform and methanol we slowly reduced pressure in 5 mbar increments to reach a gentle boiling point of solution. After reaching the final pressure of 55 mbar, we incubated the solution at reduced pressure for 2 min. In the next step, we separated vesicle fraction from the aqueous solution and excess fluorescein with centrifuging at 15700x g for 10 min. Lipid vesicles in the pellet were resuspended in 40 mL, 10 mM HEPES buffer. We washed lipid vesicles three times, and after the third time vesicles were concentrated into 5 mL HEPES buffer. For all experiments, the vesicles were freshly prepared. Lipid vesicle size was determined with DIC and FL microscopy.

2.2. Preparation of surfactin solution

Surfactin solution was prepared in 10 mM HEPES buffer solution at a concentration of 1 mg/ml (Surfactin sodium salt, Fujifilm Wako Pure Chemical Corporation, USA). The stock solution was then diluted to the desired concentration and added to the vesicle solution.

2.3. Turbidity assay

A turbidity assay was performed as described by Ahyayauch et al. [20]. Briefly, in a 96-well microtiter plate, 90 μL of vesicle solution was mixed with 10 μL of surfactin serial dilution. The final detergent concentration gradient ranged from 0.03 to 1.7 mM. The mixtures were left to equilibrate for 10 min, and solubilization was assessed from the changes in turbidity (Optical Density at 650 nm; OD650). Measurements

were made with a Biotek Cytation 3 microplate reader (BioTek, Winooski, VT). Experiments were performed at room temperature (23 °C) and 60 °C where samples were pre-heated prior to mixing, incubation and measurement.

2.4. Microscopy

DOPC GVs were exposed to surfactin under the microscope and monitored online to capture early lipid vesicle dynamics. In the experiments, the concentration of GVs was between 10^6 and 10^7 vesicles/mL. 9 μL of vesicle suspension was pipetted onto a #1.5 microscope cover-glass to form a hemispheric drop. After positioning and focusing the vesicle suspension on the microscope, 1 μL of appropriate surfactin solution was added. Image acquisition started right after the addition of surfactin. Dynamics of lipid solubilization with surfactin was visualized with fluorescence microscope Zeiss Axio Observer Z1 equipped with confocal unit LSM 800 (Carl Zeiss, Oberkochen, Germany). Fluorescein stain was excited with 488 nm laser wavelength and emission spectrum of 500–700 nm was acquired. Additionally, samples were visualized with differential interference contrast (DIC) technique. The image acquisition was done with an immersion oil 100x objective. Because the vesicles were undergoing Brownian motion and occasionally went out of focus, manual vesicle tracking was needed to acquire the full sequence of vesicle dynamics. The experiments were made under ambient conditions (room temperature, ambient air pressure) and at 60 °C with heating insert (Pecon, P-LabTek S1) and preheated vesicles and surfactin solutions on a block heater (SBH130DC, Stuart, UK). Consecutive image acquisition with DIC and FL technique was performed up to 7 min after surfactin addition or up to full vesicle solubilization. Time lapse microscopic images were acquired in 0.45 s and 0.32 s time step per frame for DIC and FL techniques, respectively.

The individual vesicles were imaged at multiple z-plane positions to obtain series of images at different depths (z-stack). The z-stack acquisition was used in successive repeats to obtain z-stack images at different times after addition of surfactin.

2.5. Image analysis

For the microscopic image analysis, ImageJ software (1.53f) [21] was used. For the determination of vesicle intensities, the individual vesicles in time series were aligned (plugin.

“Align images in stack”), then the region of interest (ROI) was cropped and the thresholded image was analyzed with plugin “Analyze particles” to obtain GV intensities of the individual microscopic images. As vesicle shape visualization of z-stack images were acquired in 0.3 μm thin sections with total stack height up to 4.2 μm with total acquisition time of approximately 6.1 s. Image post-processing was done with ImageJ software (1.53f). Firstly, images were trimmed to smaller ROI to obtain the single vesicle. As vesicles were freely moving in the suspension, the individual vesicle was aligned in stack with plugin “Align images in stack” with selected vesicle as ROI. Realigned images were further used for 3D vesicle shape reconstruction, where ImageJ plugin 3D viewer was used. The 3D model was presented as a volume mode or surface mode with smoothing parameter set to value 20.

3. Monte Carlo simulations of surfactin interactions with lipid bilayers

We modeled a lipid vesicle with a triangular mesh composed of N vertices connected by tethers that form a self-avoiding closed network [10,22]. The Monte Carlo scheme is based on the minimization of bending energy with a heterogeneous membrane composed of flat and inherently negatively curved patches. The details of the model are given in [Supplementary Information A](#).

4. Results

4.1. Experimental results

Effect of surfactin on DOPC GVs is given in Fig. 2 with optical density (OD_{650}) measurements. The CMC was determined to be 33 μM by measurement of surface tension (for details see Supplementary Information). Below 10 μM concentration, surfactin had no substantial effect on vesicles. At around 33 μM concentration (CMC), OD_{650} decreased approximately to 80% of their initial value. Increasing the concentration above CMC resulted in marked exponential decrease of OD_{650} values as expected. At 1000 μM concentration, the OD_{650} values substantially decreased to only a few percent of their initial value.

The effect of surfactin on the cloudiness or opacity of a solution (turbidity) caused by suspended vesicles was found to be consistent at both elevated temperature (60 °C) and room temperature. The decrease in turbidity could not be attributed solely to vesicle solubilization, as it could also result from changes in vesicle size and shape [23]. To further explore surfactin’s impact on DOPC GVs, we employed the DIC technique to examine the vesicles. Introducing surfactin to the GV solution resulted in noticeable dynamic changes in topology. At a surfactin concentration of 10 μM (sub CMC concentration), the vesicle topology remained largely unaffected. However, when surfactin concentrations reached 100 μM or higher (above CMC), significant alterations in vesicle shape and topology became apparent. The most striking topological change was the appearance of darker invaginated areas on the surface of the vesicles (Fig. 2). As the surfactin concentration increased (100 μM , 500 μM , and 1000 μM), the number of these invaginated areas grew substantially. At concentrations above 100 μM , the invaginations were seen to combine and form larger, crater-like structures on the vesicle surface (Fig. 2). The results demonstrate that invagination always precedes solubilization and that solubilization can lead to the decrease of OD values (i.e. vesicle solubilization was completed in few minutes,

whereas turbidimetric measurements were performed after 10 min incubation when system reached equilibrium). An additional time sequence of DIC and FL images is available in Supplementary Information.

To get a better 3D view of topological changes induced by the addition of surfactin, we have fluorescently labeled the vesicles’ lumen and observed the GVs with FL. A typical decrease in vesicle fluorescence intensity with corresponding confocal laser scanning microscopic images is shown in Fig. 3(a). Vesicle fluorescence intensity drops after 30 s of surfactin addition, likely due to leakage of the vesicle lumen. Similarly to DIC microscopic images, addition of surfactin caused a formation of dark indented structures which had low fluorescence intensity (in Fig. 3(a) at 50 s time). The rate of decrease of fluorescence intensity (Fig. 3(b)) was dependent on surfactin concentrations. Increased surfactin concentration induces faster decline in fluorescence intensity (see detailed analysis in Figures S2 and S3 in Supplementary Information B). At 10 μM surfactin concentration, the vesicles appeared stable on the order of minutes. In contrast at 1000 μM surfactin vesicle solubilization was too fast to capture under the microscope. In the absence of surfactin addition the fluorescence intensity decreased slowly and approximately linearly. The results demonstrate that invagination always precedes solubilization and that solubilization can lead to the decrease of OD_{650} values (i.e. vesicle solubilization was completed in few minutes, whereas turbidimetric measurements were performed after 10 min incubation when system reached equilibrium). An additional time sequence of DIC and FL images is available in Supplementary Information.

To follow the membrane invaginations into the lipid vesicle a series of microscopic z-axis images of a single vesicle were stacked with ImageJ software (1.53f) to reconstruct a 3D vesicle shape. For samples with no added surfactin, the 3D reconstructions of the vesicles appear smooth and homogeneous for both temperatures (Fig. 4(a-f)). With the addition of surfactin, dark spots (pit-like membrane invaginations) begin appearing in the 3D reconstituted vesicles (Fig. 4(g-i)). The 3D

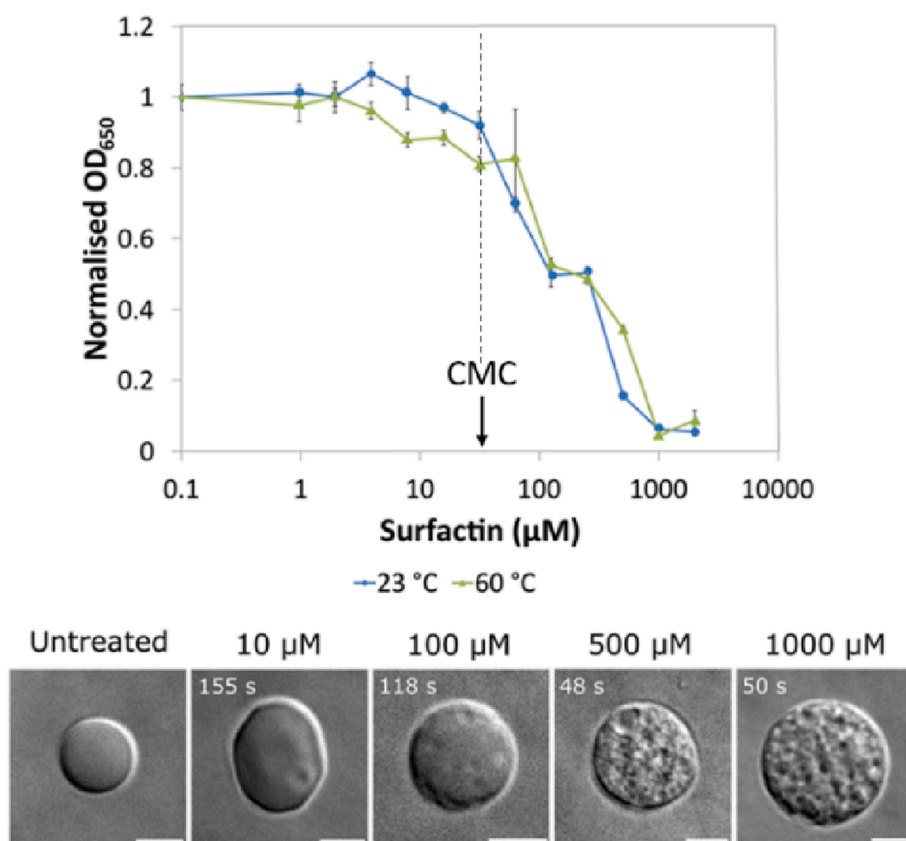


Fig. 2. The turbidity assay was conducted to evaluate the impact of surfactin on DOPC giant vesicles (GVs). A consistent decrease in optical density (OD_{650}) was observed as surfactin concentrations increased, with measurements taken at both 23 °C and 60 °C, represented by blue and green lines, respectively. The error bars display the standard deviation from three repeated experiments at each temperature ($n = 3$). Microscopic images captured at 23 °C reveal vesicle structures at specified concentrations and time intervals following surfactin exposure. Note the change in the decrease of OD_{650} before and after CMC (33 μM), which was calculated using surface tension (see Supplementary Information). Higher surfactin concentrations led to a greater number of membrane invaginations. Scale bar: 5 μm .

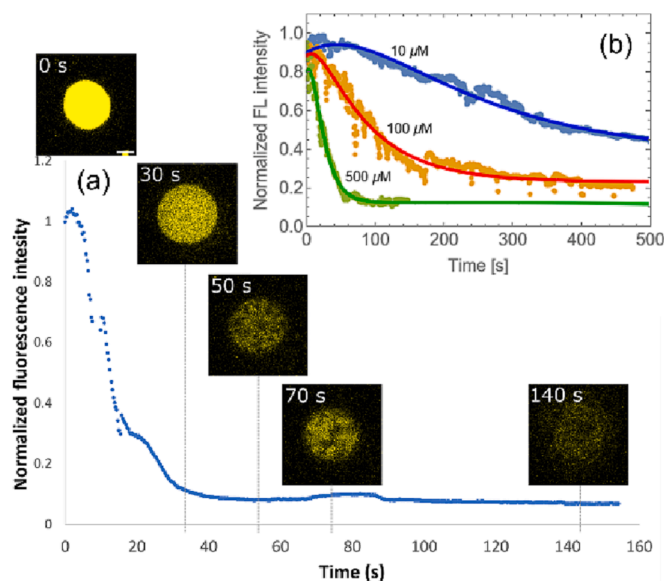


Fig. 3. Fluorescence intensity of vesicles decreases with time and surfactin concentration. (a): Fluorescence intensity curve of a vesicle at 23 °C measured in a typical experiment. Surfactin was added at $t = 0$ at concentration 500 μM . Accompanying microscopic images illustrate the development of dark regions preceding the solubilization of the vesicle. A 5 μm scale bar is included in the micrographs for reference. (b) The rate of average fluorescence intensity reduction is more rapid at elevated surfactin concentrations. In this case, the data points signify the average results from four experiments, while the lines represent the optimal fit according to the compartment model for fluorescence decline detailed in Supplementary Information B.

time evolution of membrane invaginations for a given lipid vesicle is given in Fig. 4(j-k). The first deviations from the spherical shapes at room temperature are seen already after 18 s. The number of membrane invaginations increased with time. The invaginations were metastable up to 60 s at room temperature.

At temperatures of 60 °C, less pronounced membrane invaginations were observed, possibly due to the system having more thermal energy, impeding the integration of surfactin molecules into the GV membranes across the whole system. Additionally, short chain amphiphiles like surfactin might reduce the membrane rigidity by reduction of curvature frustration, rendering membranes at room temperature to be softer and more prone to buckling [24,25]. It is also possible that higher temperatures induce an increased flip-flop of surfactin molecules into the inner monolayer like observed in SDS, but research on this topic is lacking [26].

4.2. Simulation results

The results of the simulations are summarized in Fig. 4(l-m). The vesicles are simulated with a triangular mesh that is self-avoidant (details are given in Supplementary Information A). Essentially, each vertex can consist of either a flat membrane or a membrane nanodomain (ND) with a preferred dimensionless spontaneous curvature c_0 . The parameter of spontaneous curvature is an effective one, meaning it can encompass ND shapes as well as area differences between two monolayers of lipids arising from the preferential embedding of surfactin aggregates in the outer monolayer (see Supplementary Information A for a detailed derivation). Prior to every simulation, relative temperature T/T_0 and relative ND density ρ are set. To simulate smoother membranes at elevated temperatures (thought to be induced by flip-flop of NDs into the inner monolayer), c_0 dependence on temperature is approximated by a linear relationship $c_0(T) = T/2T_0 - 1$, where $T_0 = 300$ K. Snapshots of typical simulation results at $\rho = 0.3$ and different temperatures are shown in Fig. 4(m). With decreasing temperature, invaginations start to form

on the vesicles.

Simulations at high temperatures T/T_0 return quasi-spherical vesicles with no visible indentations at all ranges of ρ . These cases in the $T/T_0(\rho)$ diagram are labelled as the smooth regime. When more NDs aggregate to form a larger domain, invaginations start appearing on the vesicles, indicating a transition to an invaginated regime (at low T/T_0 and all ρ). The line separating the phase separation between the Smooth and Invaginated regimes is marked S-I on Fig. 4(l). This transition has a maximum around $\rho = 45\%$.

Once the vesicles are in the Invagination regime, decreasing T/T_0 or increasing ρ leads to an increased number of invaginations on the vesicle. The number of invaginations per vesicle in Fig. 4(l) is denoted by the number in brackets. For example, a vesicle with a total of 8 invaginations is labeled as I(8).

For a qualitative measure of the ND cluster size we measure the average number of NDs included in clusters by [22]:

$$\langle \bar{N}_{vc} \rangle = \left\langle \frac{\sum_i N_{vc}^{(i)} N_{cl}^{(i)}}{\sum_i N_{cl}^{(i)}} \right\rangle \quad (1)$$

Here, the angle brackets \bar{N}_{vc} denote the canonical ensemble average, \bar{N}_{vc} is the mean cluster size with the sums running over all clusters of vertices representing NDs. In the sums, $N_{vc}^{(i)}$ is the number of vertices in cluster i and $N_{cl}^{(i)}$ is the number of clusters of size $N_{vc}^{(i)}$. The average cluster size of ND is given by a heat map in Fig. 4(m) and is a monotonously increasing function of ρ . ND clusters are smallest at higher temperatures where mixing of NDs and lipids.

is most preferred by configurational entropy. Conversely we observe that lower temperatures promote clustering and the formation of invaginations.

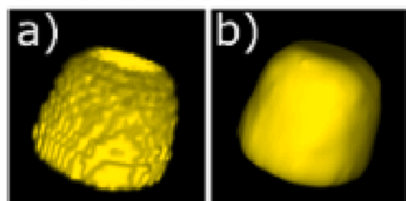
Interestingly, two regions of largest clusters in the $T - \rho$ space are separated by a small gap in the region where T/T_0 is 0.85 and ρ is 45% to 50%. This may be due to the membrane invaginations not being fully formed with the majority of NDs still distributed homogeneously across the vesicle.

5. Discussion

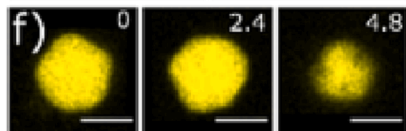
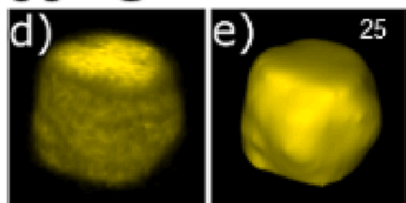
The impact of surfactin on lipid membranes has been previously discussed in an indirect manner, but to the best of our knowledge, there have been no prior observations of surfactin-induced invaginations in the lipid membranes of giant vesicles (GVs). Thermodynamic experiments by Yuan et al. [7] revealed that even minimal concentrations of surfactin can impede membrane fusion. Additionally, a computational analysis by Grau et al. [13] demonstrated that the integration of surfactin into the bilayer alters the membrane's curvature. Heerklotz and Seeliger proposed a solubilizing effect of surfactin based on their isothermal titration calorimetry experiments [4]. In their dehydration-fluidization model, surfactin molecules, which possess an intrinsic conical shape, experience a geometric mismatch when inserted into the flat lipid bilayer. This discrepancy is compensated by the headgroup's compression (dehydration) and lateral expansion of the hydrocarbon chain (fluidization) [14]. Consequently, a surfactin molecule with a conical structure can induce the formation of a membrane nanodomain with negative spontaneous curvature since its neighboring lipids become inverted-conical (see Fig. 1). This effect becomes less significant (i) as the temperature increases, and (ii) as the surfactin content in the membrane decreases. This hypothesis forms the basis of the present study. It is crucial to avoid misconstruing the concept of monolayer curvature with that of bilayer curvature. The observed membrane curvature is an outcome influenced by both monolayers and while an individual monolayer can exhibit positive spontaneous curvature, it is essential to recognize that the total spontaneous curvature of a bilayer is ultimately zero.

Utilizing differential interference contrast (DIC) and fluorescence (FL) microscopy, our observations revealed that the integration of

Untreated



60 °C



23 °C

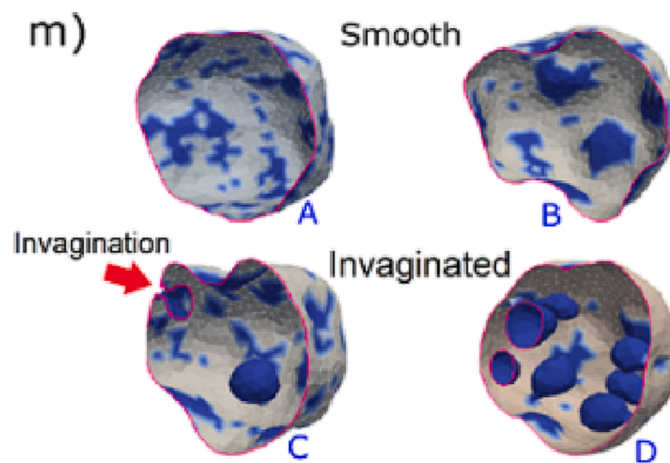
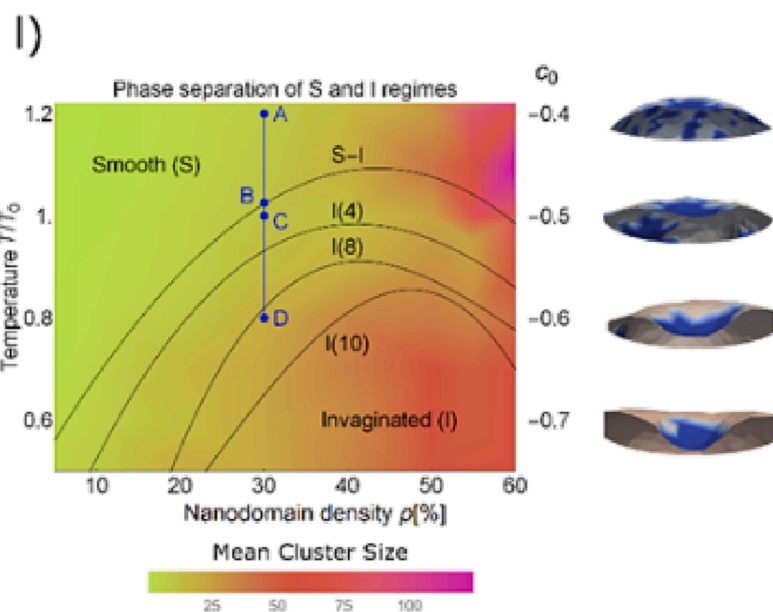
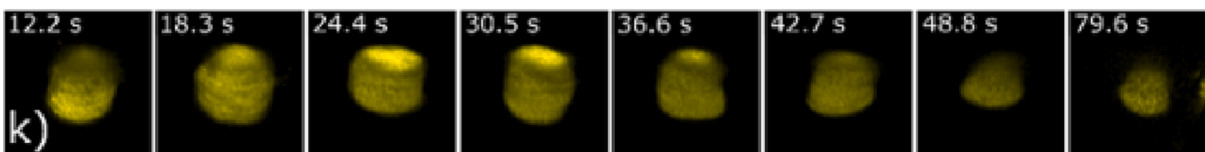
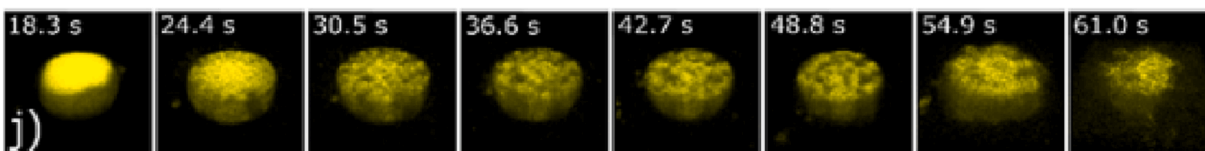
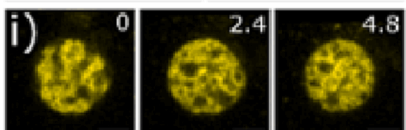
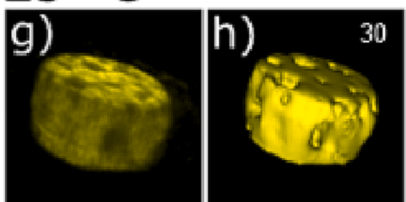


Fig. 4. Time evolution of 3D reconstructions of DOPC GV incubated with 500 μM surfactin and Monte Carlo simulation results. Panels (a), (d), (g), (j) and (k) shows vesicle 3D reconstructions of volume and panels (b), (e) and (h) show 3D reconstructions of vesicle surfaces. Panels (c), (f) and (i) show microscopic 2D images at different positions of z-axis in μm (upper right corner of each panel). Panels (j) and (k) show 3D vesicle reconstructions at temperatures 23 $^{\circ}\text{C}$ and 60 $^{\circ}\text{C}$, respectively, after an addition of (500 μM) surfactin. Panel (l) shows the phase diagram of simulations in the temperature-density plane. The spontaneous curvature c_0 of membrane nanodomains (NDs) is directly proportional to the temperature. The four points A, B, C and D in the phase diagram correspond to typical shapes of simulated vesicles shown in panel (l). The S-B line separates the Smooth and Invaginated regimes; point C in the phase diagram shows the inception of an invaginated structure denoted by the red arrow. The color gradient corresponds to the mean cluster size of inclusions defined by equation (1). Panel (m): typical snapshots of Smooth and invaginated simulated vesicle shapes that correspond to points on panel (l).

surfactin molecules into the lipid bilayer of DOPC GVs at concentrations below solubilization thresholds impact the GVs in two unique ways. First, GVs exposed to surfactin at room temperature maintain their stable structures up to several minutes, even at elevated surfactin levels (10–500 μM). This indicates surfactin's capacity to temporarily stabilize the GVs before complete solubilization, contrasting with other detergents known to induce rapid and dynamic shape alterations in GVs [9,10]. Second, 3D GV analysis shows the presence of enduring membrane invaginations (at surfactin concentrations exceeding 100 μM) that persist for minutes prior to solubilization.

The formation and stability of these membrane invaginations are not easily understood due to surfactin's conical molecular shape (Fig. 1). In contrast, another cone-shaped detergent, Triton X-100 (TR), induces noticeable exvaginations in GV membranes [10]. This distinct difference could potentially be explained by the presence of peptide bonds in surfactin's polar headgroup, making it considerably more rigid than the more flexible headgroup found in TR. Additionally, the lengthy acyl chain in surfactin, absent in TR, may anchor the molecule deeply into the outer lipid monolayer [7], influencing the surrounding lipids in accordance with Heerklotz et al.'s dehydration-fluidization model (see Fig. 1) [14].

Experimental observations and molecular dynamics simulations have demonstrated the presence of surfactin-lipid domains [13,27,12]. These domains may potentially aggregate and form a larger, macro domain that can be detected using microscopy techniques through depletion and fluctuation mechanisms [15,28,29]. Besides hydrophobic mismatch [28], lipids near membrane-embedded surfactin molecules undergo tilt and stretching deformations, leading to lipid-mediated interactions via depletion forces [16,30]. As two surfactin molecules approach each other within the membrane, the number of distorted lipids between them decreases, possibly generating a lipid-mediated attractive force [15,28].

We propose that elevated temperatures influence surfactin's impact on GVs through several distinct mechanisms. In experiments conducted at temperatures of 60 °C, the system exhibits a higher level of thermal energy, leading to increased Brownian motion of surfactin molecules and possible hindered integration of surfactin molecules into GV membranes due to entropic mixing. This might result in overall decreased nanodomain formation. According to the theoretical calculations conducted by Szeifer et al. [24], there is a significant reduction in the bending rigidity of membranes as the average area per chain increases (which indeed happens when surfactin fluidizes the acyl chains of DOPC lipids (see Fig. 1). This reduction also occurs when there is a decrease in curvature frustration, such as through the introduction of short chain amphiphiles (such as surfactin). In simpler terms, the available research suggests that when the area per molecule increases or when the presence of short chain amphiphiles reduces curvature frustration, there is a notable decrease in the bending rigidity of the membranes. In our case, the effect of decreased membrane rigidity is two-fold (are per lipid larger and short chain surfactin insertions reduce curvature frustration), prompting easier buckling of the surfactin-lipid nanodomains in the membrane at room temperatures [25].

An enhanced flip-flop rate at higher temperatures is also possible: at elevated temperatures, experiments show an accelerated rate of flip-flop of SDS into the inner lipid monolayer [26]. If this were the case with surfactin, dehydration and fluidization would occur simultaneously in both leaflets, leading to the formation of curved nanodomains on each side. These nanodomains then balance out to create a nearly zero membrane curvature on the exterior, which aligns with our observation of smooth GV populations at 60 °C.

Additionally, higher temperatures result in thinner membranes. Studies on DOPC vesicles have demonstrated a more than two-fold reduction in membrane thickness when the temperature increases from 22 °C to 60 °C [31]. The combination of these effects may create a positive feedback loop, which could explain the lack of membrane invaginations in GVs at elevated temperatures, but more conclusive

research is necessary to confirm these claims.

To enhance our understanding of the temperature-dependent nature of this phenomenon, we conducted numerical Monte Carlo simulations focusing on the behavior of closed membrane structures. The modeled vesicles incorporated flat membrane patches devoid of spontaneous curvature, as well as regions displaying negative spontaneous curvature. The surfactin-lipid nanodomains were represented by patches of negative spontaneous curvature. To simulate the formation of surfactin-surfactin or surfactin-lipid domains as observed in experimental settings, these patches could interact with each other through a variable interaction to mimic the formation of surfactin-surfactin or surfactin-lipid domains observed in experiments [3,13,27,32,33]. Interestingly, our numerical findings reveal that the occurrence of membrane invaginations in our model demonstrates an inverse relationship with temperature, thereby reinforcing the initial dehydration-fluidization hypothesis.

Membrane invaginations could have physiological implications, such as affecting vesicle formation, endocytosis, and exocytosis processes, which are crucial in cellular transport and communication. Furthermore, surfactin has antiviral activity and topological changes of viral envelope could interfere with viral infectivity [7]. However, other effects like solubilization of membranes and leakage of fluorescein, may also have physiological consequences, like disrupting membrane integrity and altering cellular permeability. Thus, while invaginations might have specific physiological roles, it is crucial to consider the broader context of all surfactin-induced effects on lipid bilayers and GVs to understand their full implications. Further research is needed to clarify the physiological significance and roles of these effects in a biological context.

6. Conclusion

We investigate the interaction between DOPC giant vesicles (GVs) and surfactin at concentrations below its solubilization threshold, using differential interference contrast (DIC) and fluorescence (FL) microscopy. The experiments were conducted at both room temperature (23 °C) and elevated temperature (60 °C). Our 3D vesicle reconstructions reveal invaginated membrane patches on the GV surfaces, which are more prevalent at lower temperatures.

These membrane invaginations are hypothesized to result from surfactin's solubilizing action as it incorporates into the outer lipid layer's lamellar packing. The cone-shaped geometry of surfactin causes the nearby lipids to dehydrate in their headgroup regions and become more fluid in their tail regions (Fig. 1). This process forms a surfactin-lipid nanodomain with an overall negative spontaneous curvature. It is believed that these nanodomains cluster to create the macroscopic membrane invaginations observed in the experiments (Fig. 2, bottom right).

As temperature increases, the higher thermal energy and increased Brownian motion of surfactin molecules hinder their integration into the membranes of GVs due to increased entropic mixing. Theoretical calculations support the idea that as the average area per chain increases (as seen when surfactin fluidizes the acyl chains of DOPC lipids), the bending rigidity of the membranes significantly reduces. This reduction in rigidity is also observed when curvature frustration decreases, such as through the presence of short-chain amphiphiles like surfactin. The combined effects of increased area per lipid and reduced curvature frustration in the presence of surfactin make the surfactin-lipid nanodomains in the membrane more susceptible to buckling at room temperature. Additionally, accelerated flip-flop rate of surfactin into the inner lipid monolayer at elevated temperatures may lead to a less negative spontaneous curvature of surfactin containing membrane patches. Theoretically, equal numbers of surfactin-lipid nanodomains in both membrane lipid layers would result in a net zero membrane spontaneous curvature and smooth vesicles. To validate these hypotheses, we conducted numerical Monte Carlo simulations of closed vesicle

shapes featuring patches of negative spontaneous curvature on the membrane. The simulation results align well with experimental observations and provide a potential explanation for the inverse relationship between membrane invaginations and temperature.

CRedit authorship contribution statement

Žiga Pandur: Methodology, Validation, Formal analysis, Investigation, Writing – original draft, Writing – review & editing, Visualization. **Samo Penič:** Methodology, Software. **Aleš Igljič:** Methodology, Validation, Resources, Data curation, Writing – review & editing, Supervision, Funding acquisition. **Veronika Kralj-Igljič:** Methodology, Validation, Resources, Data curation, Writing – review & editing, Supervision, Funding acquisition. **David Stopar:** Methodology, Validation, Resources, Data curation, Writing – review & editing, Supervision, Funding acquisition. **Mitja Drab:** Methodology, Software, Formal analysis, Investigation, Visualization, Writing - original draft, Writing - review & editing.

Declaration of Competing Interest

The authors declare that they have no known competing financial interests or personal relationships that could have appeared to influence the work reported in this paper.

Data availability

Data will be made available on request.

Acknowledgements

This research was financed by the Research programs P2-0232, P3-0388, P4-0116 and Research projects J2-4447 and J3-3066, all from the Slovenian Research Agency (ARRS). The authors would like to acknowledge fruitful discussions with Prof. Nir Gov and Yoav Ravid.

Appendix A. Supplementary data

Supplementary data to this article can be found online at <https://doi.org/10.1016/j.jcis.2023.07.057>.

References

- R. Sen, Surfactin: Biosynthesis, Genetics and Potential Applications, in: R. S. Biosurfactants (Ed.), Advances in Experimental Medicine and Biology, Springer, New York, NY, 2010, pp. 316–323, https://doi.org/10.1007/978-1-4419-5979-9_24.
- A.W. Bernheimer, L.S. Avigad, Nature and Properties of a Cytolytic Agent Produced by *Bacillus subtilis*, *Microbiology* 61 (3) (1970) 361–369, <https://doi.org/10.1099/00221287-61-3-361>.
- C. Carrillo, J.A. Teruel, F.J. Aranda, A. Ortiz, Molecular mechanism of membrane permeabilization by the peptide antibiotic surfactin, *Biochimica et Biophysica Acta (BBA) - Biomembranes* 1611 (1) (Apr. 2003) 91–97, [https://doi.org/10.1016/S0005-2736\(03\)00029-4](https://doi.org/10.1016/S0005-2736(03)00029-4).
- H. Heerklotz, J. Seelig, Detergent-like action of the antibiotic peptide surfactin on lipid membranes, *Biophys. J.* 81 (3) (Sep. 2001) 1547–1554, [https://doi.org/10.1016/S0006-3495\(01\)75808-0](https://doi.org/10.1016/S0006-3495(01)75808-0).
- H. Heerklotz, J. Seelig, Leakage and lysis of lipid membranes induced by the lipopeptide surfactin, *Eur. Biophys. J.* 36 (4) (Apr. 2007) 305–314, <https://doi.org/10.1007/s00249-006-0091-5>.
- G. Henry, M. Deleu, E. Jourdan, P. Thonart, M. Ongena, The bacterial lipopeptide surfactin targets the lipid fraction of the plant plasma membrane to trigger immune-related defence responses, *Cell. Microbiol.* 13 (11) (2011) 1824–1837, <https://doi.org/10.1111/j.1462-5822.2011.01664.x>.
- L. Yuan, S. Zhang, Y. Wang, Y. Li, X. Wang, Q. Yang, Surfactin Inhibits Membrane Fusion during Invasion of Epithelial Cells by Enveloped Viruses, *J. Virol.* 92 (21) (Oct. 2018) e00809–e818, <https://doi.org/10.1128/JVI.00809-18>.
- H. Heerklotz, T. Wierprecht, J. Seelig, Membrane Perturbation by the Lipopeptide Surfactin and Detergents as Studied by Deuterium NMR, *J. Phys. Chem. B* 108 (15) (Apr. 2004) 4909–4915, <https://doi.org/10.1021/jp0371938>.
- M. Nazari, M. Kurdi, H. Heerklotz, Classifying Surfactants with Respect to Their Effect on Lipid Membrane Order, *Biophys. J.* 102 (3) (Feb. 2012) 498–506, <https://doi.org/10.1016/j.bpj.2011.12.029>.
- M. Drab, Ž. Pandur, S. Penič, A. Igljič, V. Kralj-Igljič, D. Stopar, A Monte Carlo study of giant vesicle morphologies in nonequilibrium environments, *Biophys. J.* 120 (20) (Oct. 2021) 4418–4428, <https://doi.org/10.1016/j.bpj.2021.09.005>.
- F. Francius, S. Dufour, M. Deleu, M. Paquot, M.-P. Mingéot-Leclercq, Y.F. Dufrène, Nanoscale membrane activity of surfactins: influence of geometry, charge and hydrophobicity, *Biochim Biophys Acta* 1778 (10) (Oct. 2008) 2058–2068, <https://doi.org/10.1016/j.bbame.2008.03.023>.
- M. Deleu, et al., Interaction of Surfactin with Membranes: A Computational Approach, *Langmuir* 19 (8) (Apr. 2003) 3377–3385, <https://doi.org/10.1021/la026543z>.
- A. Grau, J.C. Gómez Fernández, F. Peypoux, A. Ortiz, A study on the interactions of surfactin with phospholipid vesicles, *Biochimica et Biophysica Acta (BBA) - Biomembranes* 1418 (2) (May 1999) 307–319, [https://doi.org/10.1016/S0005-2736\(99\)00039-5](https://doi.org/10.1016/S0005-2736(99)00039-5).
- H. Heerklotz, H. Binder, G. Lantzsch, G. Klose, A. Blume, Lipid/Detergent Interaction Thermodynamics as a Function of Molecular Shape, *J. Phys. Chem. B* 101 (4) (Jan. 1997) 639–645, <https://doi.org/10.1021/jp962342q>.
- S. Marčelja, Lipid-mediated protein interaction in membranes, *Biochimica et Biophysica Acta (BBA) - Biomembranes* 455 (1) (Nov. 1976) 1–7, [https://doi.org/10.1016/0005-2736\(76\)90149-8](https://doi.org/10.1016/0005-2736(76)90149-8).
- M. Fošnaric, A. Igljič, S. May, Influence of rigid inclusions on the bending elasticity of a lipid membrane, *Phys. Rev. E* 74 (5) (Nov. 2006), 051503, <https://doi.org/10.1103/PhysRevE.74.051503>.
- N.S. Gov, V. Kralj-Igljič, R.K. Sadhu, L. Mesarec, A. Igljič, Chapter 25 - Physical principles of cellular membrane shapes, in: S. Suetsugu (Ed.), *Plasma Membrane Shaping*, Academic Press, 2023, pp. 393–413, <https://doi.org/10.1016/B978-0-323-89911-6.00025-X>.
- M. Drab, R.K. Sadhu, Y. Ravid, A. Igljič, V. Kralj-Igljič, N.S. Gov, Chapter 26 - Modeling cellular shape changes in the presence of curved membrane proteins and active cytoskeletal forces, in: S. Suetsugu (Ed.), *Plasma Membrane Shaping*, Academic Press, 2023, pp. 415–429, <https://doi.org/10.1016/B978-0-323-89911-6.00022-9>.
- A. Moscho, O. Orwar, D.T. Chiu, B.P. Modi, R.N. Zare, Rapid preparation of giant unilamellar vesicles, *Proc. Natl. Acad. Sci.* 93 (21) (Oct. 1996) 11443–11447, <https://doi.org/10.1073/pnas.93.21.11443>.
- H. Ahyayauch, M.I. Collado, A. Alonso, F.M. Goñi, Lipid Bilayers in the Gel Phase Become Saturated by Triton X-100 at Lower Surfactant Concentrations Than Those in the Fluid Phase, *Biophys. J.* 102 (11) (Jun. 2012) 2510–2516, <https://doi.org/10.1016/j.bpj.2012.04.041>.
- C.A. Schneider, W.S. Rasband, K.W. Eliceiri, NIH Image to ImageJ: 25 years of image analysis, *Nat Methods* vol. 9, no. 7, Art. no. 7 (Jul. 2012), <https://doi.org/10.1038/nmeth.2089>.
- M. Fošnaric, S. Penič, A. Igljič, V. Kralj-Igljič, M. Drab, N.S. Gov, Theoretical study of vesicle shapes driven by coupling curved proteins and active cytoskeletal forces, *Soft Matter* 15 (26) (2019) 5319–5330, <https://doi.org/10.1039/C8SM02356E>.
- A. Wang, C.C. Miller, J.W. Szostak, Interpreting turbidity measurements for vesicle studies, *bioRxiv*, p. 348904, Jun. 15, 2018. doi: 10.1101/348904.
- I. Szleifer, D. Kramer, A. Ben-Shaul, W.M. Gelbart, S.A. Safran, Molecular theory of curvature elasticity in surfactant films, *J. Chem. Phys.* 92 (11) (Jun. 1990) 6800–6817, <https://doi.org/10.1063/1.458267>.
- A.I.I. Tyler, J.L. Greenfield, J.M. Seddon, N.J. Brooks, S. Purushothaman, Coupling Behavior of Fatty Acid Containing Membranes to Membrane Bio-Mechanics, *Front. Cell Dev. Biol.* 7 (Sep. 2019) 187, <https://doi.org/10.3389/fcell.2019.00187>.
- H. Heerklotz, Interactions of surfactants with lipid membranes, *Q. Rev. Biophys.* 41 (3–4) (Nov. 2008) 205–264, <https://doi.org/10.1017/S0033583508004721>.
- M. Deleu, K. Nott, R. Brasseur, P. Jacques, P. Thonart, Y.F. Dufrène, Imaging mixed lipid monolayers by dynamic atomic force microscopy, *Biochimica et Biophysica Acta (BBA) - Biomembranes* 1513 (1) (Jul. 2001) 55–62, [https://doi.org/10.1016/S0005-2736\(01\)00337-6](https://doi.org/10.1016/S0005-2736(01)00337-6).
- K. Bohinc, V. Kralj-Igljič, S. May, Interaction between two cylindrical inclusions in a symmetric lipid bilayer, *J. Chem. Phys.* 119 (14) (Oct. 2003) 7435–7444, <https://doi.org/10.1063/1.1607305>.
- T. Sintès, A. Baumgärtner, Protein attraction in membranes induced by lipid fluctuations, *Biophys. J.* 73 (5) (Nov. 1997) 2251–2259, [https://doi.org/10.1016/S0006-3495\(97\)78257-2](https://doi.org/10.1016/S0006-3495(97)78257-2).
- M. Fošnaric, K. Bohinc, D.R. Gauger, A. Igljič, V. Kralj-Igljič, S. May, The Influence of Anisotropic Membrane Inclusions on Curvature Elastic Properties of Lipid Membranes, *J. Chem. Inf. Model.* 45 (6) (Nov. 2005) 1652–1661, <https://doi.org/10.1021/ci050171t>.
- Z.V. Leonenko, E. Finot, H. Ma, T.E.S. Dahms, D.T. Cramb, Investigation of Temperature-Induced Phase Transitions in DOPC and DPPC Phospholipid Bilayers Using Temperature-Controlled Scanning Force Microscopy, *Biophys. J.* 86 (6) (Jun. 2004) 3783–3793, <https://doi.org/10.1529/biophysj.103.036681>.
- "Infrared Nanospectroscopy of Phospholipid and Surfactin Monolayer Domains | ACS Omega." <https://pubs.acs.org/doi/full/10.1021/acsomega.7b01931> (accessed Mar. 31, 2023).
- M. Deleu, et al., Effects of surfactin on membrane models displaying lipid phase separation, *Biochimica et Biophysica Acta (BBA) - Biomembranes* Feb. 2013 (2) (1828) 801–815, <https://doi.org/10.1016/j.bbame.2012.11.007>.
- R.L. Thurmond, D. Otten, M.F. Brown, K. Beyer, Structure and packing of phosphatidylcholines in lamellar and hexagonal liquid-crystalline mixtures with a nonionic detergent: a wide-line deuterium and phosphorus-31 NMR study, *J. Phys. Chem.* 98 (3) (Jan. 1994) 972–983, <https://doi.org/10.1021/j100054a038>.